Mechanistic Insight into the Symmetric Fission of [4Fe−4S] Analogue Complexes and Implications for Cluster Conversions in Iron−Sulfur Proteins

Shuqiang Niu,[†,‡] Xue-Bin Wang,[§,||] Xin Yang,[§,||] Lai-Sheng Wang,*[,§,||] and Toshiko Ichiye*[,†,‡]

School of Molecular Biosciences, Washington State University, Pullman, Washington 99164-4660, Department of Chemistry, Georgetown University, Washington, DC, 20057-1227, Department of Physics, Washington State University, 2710 University Drive, Richland, Washington 99352, and W. R. Wiley Environmental Molecular Science Laboratory, Pacific Northwest National Laboratory, P.O. Box 999, Richland, Washington 99352

Received: March 4, 2004; In Final Form: May 25, 2004

Assembly and disassembly of protein-bound iron−sulfur clusters are involved in a wide variety of vital biological processes, ranging from biosynthesis to regulation of biological function. The study of the fission of analogue clusters can provide valuable insight into the various reaction mechanisms that can occur in proteins as well as tests of the ability of theoretical studies to interpret experiment. Previously, we observed symmetric fission of doubly charged Fe−S cluster anions, $[Fe_4S_4X_4]^{2-} \rightarrow 2[Fe_2S_2X_2]^-$ (X = SC_2H_5, Cl, Br) in the gas phase, which is surprising because four strong Fe−S bonds are being broken. Here, we report a study of the detailed fission mechanism using density functional theory in conjunction with photoelectron spectroscopic results for X = Cl. Both the experimental and theoretical results suggest that the fission daughter products are low-spin $[Fe_2S_2Cl_2]^-$ ($S = {}^1/_2$) species. However, the layered structure of the cubane would seem to indicate a mechanism that would give high-spin daughter products. Thus, we investigate the symmetric fission of $[Fe_4S_4Cl_4]^{2-}$ along two possible reaction pathways, involving high-spin and low-spin $[Fe_2S_2Cl_2]^-$ fragments, respectively. Though the high-spin channel is endothermic by 1.34 eV with a high barrier of 2.65 eV, the reaction along the low-spin fission channel is more favorable with an exothermicity of 0.53 eV and a lower barrier of 1.51 eV. Two intermediates are observed along the low-spin fission channel, a spin-localized cubane $[Fe_4S_4Cl_4]^{2-}$ cluster, which contains two valence-localized Fe^{3+} centers and two valence-localized Fe^{2+} centers, and a half-opened $[Fe_4S_4Cl_4]^{2-}$ cluster. The spin-localized cluster is crucial to breaking the four strong Fe−S bonds in the symmetric fission.

Introduction

Iron−sulfur clusters are well-known to be an important class of electron carriers in electron-transfer proteins, which are involved in a wide variety of processes in all organisms, including such essential life-sustaining processes as photosynthesis, respiration, and nitrogen fixation.[1−5] Usually, the clusters exist in electron transfer proteins in the form of one to four irons tetrahedrally coordinated by cysteine residues and inorganic sulfides. Iron−sulfur clusters also have a remarkable ability for conversion among the [2Fe−2S], [4Fe−4S], and [3Fe−4S] forms whether they are free or protein-bound, which can influence protein structure and function. In particular, conversion may be involved in delivering sulfur and possibly iron for the synthesis of other biomolecules[4−7] and in regulating a network of genes as sensors for iron, oxygen, superoxide and other molecules.[6−9]

Many of the iron−sulfur clusters found in proteins assemble spontaneously and interconvert nearly quantitatively under appropriate conditions.[4] The most common transformation is the interconversion between the cubane $[4Fe-4S]^{2+}$ and the cuboidal $[3Fe-4S]^{+}$ observed in the *Desulfovibrio gigas ferredoxin* II and the enzyme aconitase.[10,11] On the other hand, since the first example of a direct $[4Fe-4S]^{2+}$ to $[2Fe-2S]^{2+}$ conversion in the iron−sulfur protein of *Azotobacter vinelandii* nitrogenase was reported in 1984,[12] this type of conversion has been also found to function as a biosensor in living cells[13] and as the radical and sulfur sources in many biosynthetic processes.[14,15] For instance, it appears to be important for the function of fumarate nitrate reductase (FNR), which in *Escherichia coli* is a global transcription regulator that controls numerous genes required for the synthesis of components of its anaerobic respiratory pathways.[9,16] The anaerobically purified form of FNR is a dimer containing a highly oxygen-sensitive $[4Fe-4S]^{2+}$ cluster per subunit.[17] On exposure to dioxygen, these $[4Fe-4S]^{2+}$ clusters are converted to $[2Fe-2S]^{2+}$ either in vitro[13] or in vivo,[18] which decreases DNA binding and results in the dissociation to the monomeric form. The $[2Fe-2S]^{2+}$ cluster can be largely reconverted to the $[4Fe-4S]^{2+}$ form under anaerobic conditions in vitro or in vivo, and the corresponding enzymatic activity is regained. Similar conversion processes have been also observed in biotin[14] and lipoate synthases.[14b] Biotin synthase contains only $[2Fe-2S]^{2+}$ clusters when isolated under aerobic conditions, which catalyzes the last step of the biosynthesis of biotin, an essential vitamin. Although the $[2Fe-2S]^{2+}$ cluster is proposed to be the sulfur source for biotin synthesis, absorption and resonance Raman studies show that the two reduced $[2Fe-2S]^{2+}$ clusters may dissociate from the protein and reassemble as a $[4Fe-4S]^{2+}$ cluster in the absence of additional iron and sulfide.[14a] Although these show that the conversion between $[4Fe-4S]^{2+}$ and $[2Fe-2S]^{2+}$ is a reversible process, the reaction mechanisms still remain unknown.

* To whom correspondence should be addressed. E-mail: (T.I.) ti9@georgetown.edu; (L.S.W.) ls.wang@pnl.gov.
† School of Molecular Biosciences, Washington State University.
‡ Georgetown University.
§ Department of Physics, Washington State University.
|| Pacific Northwest National Laboratory.

10.1021/jp049012n CCC: $27.50
Published on Web 07/21/2004

SCHEME 1

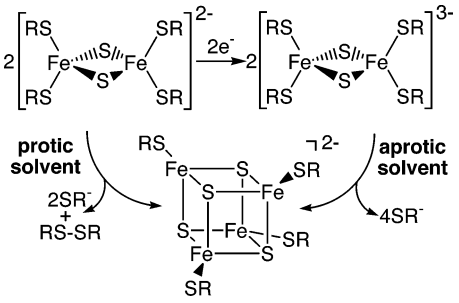

Determining the electronic structure, energetics, and interconversion mechanisms of the iron−sulfur clusters is crucial to understand the properties and function of the iron−sulfur proteins. The intrinsic thermodynamic and kinetic studies of iron−sulfur cluster assembly/disassembly in proteins are relatively challenging using quantum mechanical (QM) approaches. Given the complexity of the reaction of the clusters in the protein environment, it is essential to prove that our computational methods can predict the physicochemical properties of simple clusters in the gas phase for which we have accurate experimental values. Although recent progress in combined quantum mechanical/molecular mechanical (QM/MM) methods[19a] may lead to information about protein environmental effects on the redox active sites,[19b] the approximations made in treating the linkage between the QM and MM region necessitate careful studies of the isolated clusters beforehand. In previous synthetic studies,[20] two possible reaction pathways of $[2Fe-2S]^{2+}$ to $[4Fe-4S]^{2+}$ have been proposed on the basis of measurements of chemical and electrochemical interrelationships of one- to four-iron synthetic analogues. The conversion proceeds either by spontaneous reactions in protic media or through a reduced $[2Fe-2S]^{+}$ complex in aprotic solvent, as shown in Scheme 1. Both involve a reduced iron site per $[2Fe-2S]^{2+}$. To explore the intrinsic energetics and electronic structures of iron−sulfur clusters, we have carried out a series of investigations using a combination of techniques including electrospray ionization (ESI), photoelectron spectroscopy (PES), and density functional theory (DFT) calculations.[21−25] Although the reactions in the proteins may be influenced by the protein environment of the clusters, careful experimental and theoretical studies of analogue complexes can provide insight into possible reaction mechanisms as well as tests of the theoretical studies to interpret experiment.

A key question in these studies is the formation and the dissociation of the strong Fe−S bonds. In previous studies of the electronic structure and reduction potentials of the rubredoxin redox site analogues, $[Fe(SCH_3)_4]^{n-}$ (n = 0, 1, 2) and $[Fe(SCH_3)_3]^{n-}$ (n = 0, 1),[25] we have shown a thermodynamic cycle that relates the $[Fe(SCH_3)_3]^{-/0}$ couple and the ligand association reaction, $[Fe(SCH_3)_3]^{0/-} + SCH_3^- \rightarrow [Fe(SCH_3)_4]^{-/2-}$. Our studies showed that the $[FeX_3]^-$ and $[FeX_4]^-$ (X = Cl, Br, SCH_3) are the most stable states, because the high-spin Fe^{II} site favors a planar three-coordinated structure, whereas the high-spin Fe^{III} site favors a tetrahedral four-coordinated one.[24,25] Thus, it appears that the $Fe^{II} \leftrightarrow Fe^{III}$ conversion through an electron transfer is a crucial factor in determining the formation and breaking of Fe−S bonds in the iron−sulfur clusters in the gas phase.

More recently, we observed symmetric fission in a series of doubly charged [4Fe−4S] complexes, $[Fe_4S_4X_4]^{2-}$ (X = Cl, Br, SC_2H_5), through collision-induced dissociation (CID) and PES experiments.[20,21] The observation of the symmetric fission was unexpected because it involves breaking four strong Fe−S bonds. Our prior PES results and DFT calculations of the cubelike $[Fe_4S_4X_4]^{2-}$ complexes and the fission products $[Fe_2S_2X_2]^-$ demonstrated: (i) the parent and the fission species had similar electronic structures, owing to the unique layered structure of the $[Fe_4S_4X_4]^{2-}$ cluster and its antiferromagnetic coupling, (ii) the fission may proceed either along a high-spin channel or a low-spin channel according to Scheme 2, and (iii) the low-spin fission channel was almost thermoneutral with an endothermicity of only 0.09 eV, whereas the high-spin fission channel had a much higher endothermicity of 1.26 eV.[22] The stability of the low-spin product is not surprising because previous experimental[26] and theoretical[27,28] studies of the reduced $[Fe_2S_2R_4]^{3-}$ species showed that the $[2Fe-2S]^{1+}$ core contains a valence-localized Fe^{3+} site and a valence-localized Fe^{2+} site with a net spin $S = {}^1/_2$. On the other hand, the first example of a synthetic or biological $[Fe_2S_2]^+$ cluster with an $S = {}^9/_2$ ground state has been observed in spectroscopic studies of the Cys56Ser mutant [2Fe] ferredoxin from *Clostridium pasteurianum*.[29] Despite the thermodynamic favorability of the low-spin species, the layered structure of $[Fe_4S_4X_4]^{2-}$ seemed to suggest that the high-spin channel may be more favored kinetically because of magnetic repulsion and strong electron delocalization, in addition to the electrostatic repulsion. However, the high-spin $[Fe_2S_2X_2]^-$ daughter anions were not consistent with the PES data, which suggested that the observed $[Fe_2S_2X_2]^-$ fission products had low-spin states. Consequently, a study of the fission mechanism is necessary to resolve the barrier involved.

SCHEME 2

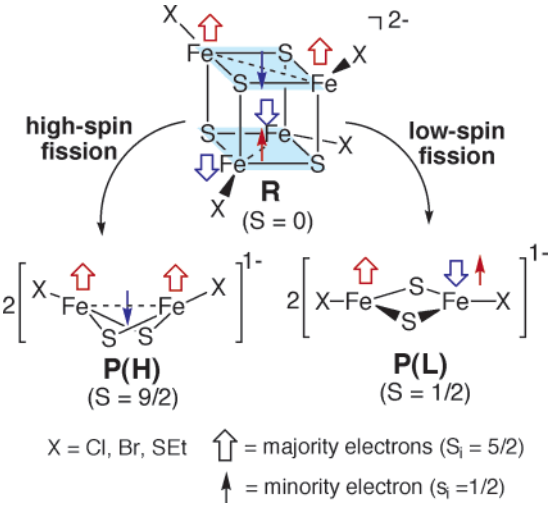

The DFT method is now a widely used computational technique to study real reaction systems containing transition metals.[30] In the current paper, we report a detailed DFT study, verified by the PES data, on the fission mechanisms of $[Fe_4S_4Cl_4]^{2-}$. This analogue has proved to be a sufficient model to obtain geometries and electronic structures of the cubane core found in the active site of the proteins because of the similarity in geometrical and electronic structure to the $[Fe(SC_2H_5)_3]^-$, $[Fe(SC_2H_5)_4]^-$, and $[Fe_4S_4(SC_2H_5)_4]^{2-}$ protein redox site analogues.[23,31] The electronic structures, geometries, and energetics of the parent and fission complexes, the intermediate complexes, and the transition states along the possible fission channels are calculated using the broken-symmetry DFT method. A major effort was made to search for transition states and intermediates along both the high-spin and low-spin fission channels. Although

no fission intermediates were found for the high-spin channel, two interesting intermediates were located for the low-spin channel, which was shown to be the favored fission channel with a significantly lower barrier. Combined with available experimental data in biological and synthetic systems, the current study provides valuable insight into iron−sulfur cluster assembly/disassembly mechanisms, as well as other enzymatic processes.

Methods

In our work on the electronic structure of $[Fe_4S_4X_4]^{2-}$ (X = SC_2H_5, SH, Cl, Br, I),[23] we have shown that although the weaker electron donor Cl ligands lead to a larger electron binding energy of $[Fe_4S_4X_4]^{2-}$ by ∼0.5 eV than the SC_2H_5 ligands, both terminal ligands lead to similar $[4Fe-4S]^{2+}$ core geometries and similar electronic structures. Therefore, in the current study, we focus on the cubane core structure for the detailed exploration of the conversion mechanism of [4Fe−4S] to [2Fe−2S] using the $[Fe_4S_4Cl_4]^{2-}$ complex as models. This avoids the necessity of exploring the conformational changes in the terminal ligands that could occur in the transition states or intermediates of $[Fe_4S_4(SC_2H_5)_4]^{2-}$.

The broken-symmetry DFT method,[32] specifically with the Becke's three-parameter hybrid exchange functional[33a−c] and the Lee−Yang−Parr correlation functional (B3LYP)[33d] using the 6-31G** basis sets,[34] was utilized for the geometry optimizations and electronic structure calculations of the iron−sulfur clusters and transition structures. An approximate spin projection procedure based on the developed method by Noodleman[35] was carried out on the broken-symmetry DFT energies of the fission reactant and products because the broken-symmetry energy of a spin polarized low-spin state is not a pure spin-state energy and is a weighted average of pure-spin states. Transition states (TS) were optimized by an eigenvalue-following optimization method,[36] in which the final updated Hessian shows only one negative eigenvalue, and were verified by several separate calculations along the reaction coordinate (RC). No symmetry restraints were imposed during geometry optimizations, and each structure was confirmed to be a ground-state structure by several separate calculations on different possible configuration states. This procedure is necessary because the electronic structure is very sensitive to the iron−sulfur cluster bonding structure. The calculated energies were refined at the B3LYP/6-31(++)$_S$G**//B3LYP/6-31G** level, where sp-type diffuse functions were added to the 6-31G** basis set of the sulfur atoms,[34,37] which significantly improved the accuracy of the calculated oxidation potentials of the iron−sulfur redox couples.[25,38] Furthermore, our recent PES and DFT studies on the tetrahedral ferric complexes $Fe^{III}X_4^-$ (X = Cl, Br) and the three-coordinate complexes $M^{II}X_3^-$ (M = Mn, Fe, Co, Ni; X = Cl, Br) have shown that increasing the basis set size for all atoms, for example, using triple-ζ basis sets, does not significantly change the calculated geometric parameters and redox energies with respect to the experimental data or the calculated values using double-ζ basis sets.[31] Self-interaction error (SIE),[39] which arises owing to the difficulty in describing the dissociation behavior of molecules with a noninteger number of electrons or spins using the DFT method, is roughly estimated for the transition states by comparing the total energy of the dissociating fragments at 40 Å with that of two separated fragments. Although the error introduced by the SIE most likely exceeds the improvement by recalculating energies at the B3LYP/6-31(++)$_S$G**//B3LYP/6-31G** level, especially for the later stages of the fission, this level is used to maintain consistency with our previous work.[25,34,37,38] In addition, because our mechanistic calculations involve the comparisons of different reaction pathways with similar dissociated fragments, the SIE tends to cancel and should not affect our conclusions.

All calculations were performed using the NWChem[40] program package. The molecular orbital visualizations were performed using the extensible computational chemistry environment (Ecce) application software.[41]

Results and Discussion

Geometries and Electronic Structures of $[Fe_4S_4Cl_4]^{2-}$ and $[Fe_2S_2Cl_2]^-$. It is well-known that the $[4Fe-4S]^{2+}$ core can be viewed as two ferromagnetic [2Fe−2S] sublayers, which are coupled antiferromagnetically to give a low-spin state.[4,7,27] The $[Fe_4S_4Cl_4]^{2-}$ (R) fission (Scheme 2) can proceed by breaking four Fe−S bonds between the two ferromagnetic sublayers to generate two high-spin $[Fe_2S_2Cl_2]^-$ daughter anions [P(H)] or within the ferromagnetic sublayers to give two low-spin $[Fe_2S_2Cl_2]^-$ daughter anions [P(L)]. The latter, however, also requires breaking the additional Fe−Fe bonding arising from the delocalization of the minority spin electrons within each sublayer. To elucidate the influence of spin states on the properties of $[Fe_4S_4Cl_4]^{2-}$ and $[Fe_2S_2Cl_2]^-$, we investigate their geometries and electronic structures by combining the DFT calculations with the PES measurements.

(a) Parent $[Fe_4S_4Cl_4]^{2-}$ Dianion (R). The electronic structure of the cubane $[4Fe-4S]^{2+}$ have been studied theoretically by Noodleman and co-workers extensively using the broken symmetry DFT methods.[27] The spin-couplings within the $[4Fe-4S]^{2+}$ core can be described by the following Heisenberg−Dirac−van Vleck (HDvV) spin Hamiltonian[27,28,42]

$$H_{spin} = J \sum_{i<j=1,4} S_i \cdot S_j \pm B(S_{AB} + {}^1/_2) \pm B(S_{CD} + {}^1/_2) \quad (1)$$

and eigenvalues

$$E(S) = (J/2)S(S+1) \pm B(S_{AB} + {}^1/_2) \pm B(S_{CD} + {}^1/_2) \quad (2)$$

where A, B, C, and D represent the four high-spin sites, J is the exchange coupling constant, B is a resonance parameter describing the delocalization in the Fe−Fe pair, S_i is the spin operator of the ith iron in $[4Fe-4S]^{2+}$, S_{ij} is the Fe−Fe pair spin operator ranging from $|S_i - S_j|$ to $S_i + S_j$ (i.e., $^1/_2$ to $^9/_2$), and S is the total spin ranging from $|S_{AB} - S_{CD}|$ to $S_{AB} + S_{CD}$ (i.e., 0−9). The spin-state energy usually represents a compromise of the competing forces between Heisenberg exchange and resonance delocalization (double exchange) in a given system.[27d] Furthermore, it was found that the $[4Fe-4S]^{2+}$ core exhibits the mixed valence state, where two high-spin Fe centers in each [2Fe−2S] sublayer are coupled ferromagnetically and one minority spin electron is delocalized between the two Fe on each sublayer, consistent with experimental observations from Mössbauer and EPR spectroscopy.[43]

The PES data and DFT calculations indicate that $[Fe_4S_4Cl_4]^{2-}$ is relatively stable with an ADE of about 0.8 eV (Table 1). Our previous studies showed that the ADEs of $[Fe_4S_4L_4]^{2-}$ (L = SH, SC_2H_5, Cl, Br, I) depend on the terminal ligands, because the HOMO's of $[Fe_4S_4L_4]^{2-}$ exhibit terminal Fe−L antibonding and strong Fe−Fe bonding character in each sublayer.[23] Similar to other ligands, in $[Fe_4S_4Cl_4]^{2-}$, the two minority electrons delocalize on the two ferromagnetic sublayers, respectively, resulting in significant intralayer Fe−Fe bonding interactions, in addition to the HDvV antiferromagnetic coupling interaction between the two ferromagnetic sublayers. As shown in Figure

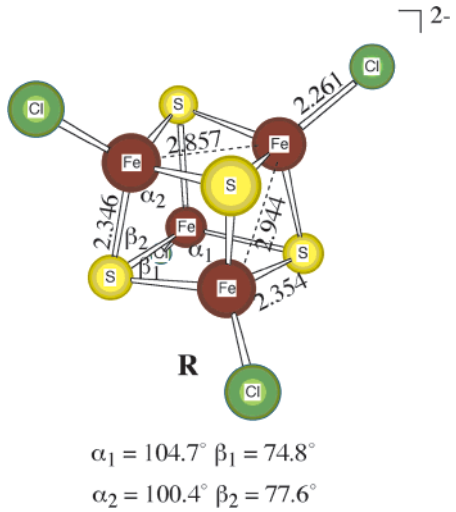

Figure 1. B3LYP/6-31G** optimized bond lengths (Å) and angles (deg) of the parent $[Fe_4S_4Cl_4]^{2-}$ dianion (R).

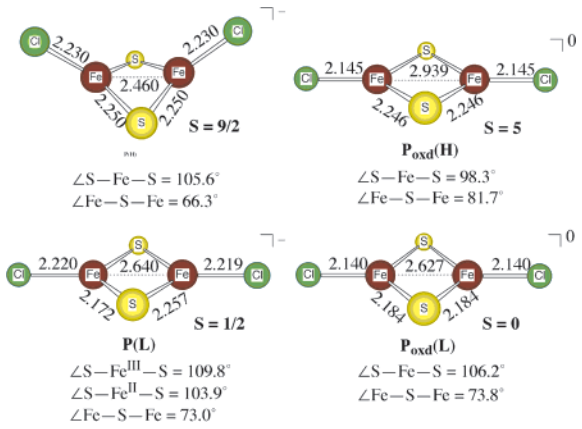

Figure 2. B3LYP/6-31G** optimized bond lengths (Å) and angles (deg) of the daughter $[Fe_2S_2Cl_2]^-$ anions, P(H) and P(L), and their oxidized states, $P_{oxd}(H)$ and $P_{oxd}(L)$.

TABLE 1: Experimental and Calculated Adiabatic (ADE) and Vertical (VDE) Detachment Energies (eV) and the Oxidant Relaxation Energies (λ_{oxd}, eV) for $[Fe_4S_4Cl_4]^{2-}$ and $[Fe_2S_2Cl_2]^-$ at B3LYP/6-31(++)$_S$G**

		ADE		VDE		λ_{oxd}	
species	S	cal	exp	cal	exp	cal	exp
$[Fe_4S_4Cl_4]^{2-}$	0	0.69	0.76	1.00	1.00	0.31	0.24
$[Fe_2S_2Cl_2]^-$	$^1/_2$	3.97	3.80	4.12	3.93	0.15	0.13
$[Fe_2S_2Cl_2]^-$	$^7/_2$	4.22		4.48		0.26	
$[Fe_2S_2Cl_2]^-$	$^9/_2$	4.09		4.73		0.64	

1, the B3LYP/6-31G** optimized Fe−Fe distance within the two sublayers of $[Fe_4S_4Cl_4]^{2-}$ is shorter by 0.087 Å. In addition, the four Fe−S bonds within each ferromagnetic layers become equal because of the effective conversion from an Fe^{2+}−Fe^{3+} pair to an $Fe^{2.5+}$−$Fe^{2.5+}$ delocalized pair. The average Fe−S bond energy in the $[4Fe−4S]^{2+}$ cubane core was estimated to be ~2 eV,[28b] close to the calculated Fe−S bond energy of the tetrahedral mono-ferric thiolate cluster.[25]

(b) High-Spin and Low-Spin $[Fe_2S_2Cl_2]^-$ Anions. Upon the fission of $[Fe_4S_4Cl_4]^{2-}$ (R), two possible $[Fe_2S_2Cl_2]^-$ daughter anions may be produced: either a high-spin product P(H) ($S = ^9/_2$) or a low-spin product P(L) ($S = ^1/_2$). As shown in Figure 2, the optimized geometry of P(L) with lowest energy has a planar structure with a valence-localized Fe^{2+}−Fe^{3+} pair, whereas the optimized geometry of P(H) with the lowest energy has a folded structure of 51° with a valence-delocalized $Fe^{2+.5}$−$Fe^{2+.5}$ pair.

TABLE 2: Calculated Charges and Net Spin Densities at the B3LYP/6-31G Level for the Parent $[Fe_4S_4Cl_4]^{2-}$ Dianion (R), the Daughter $[Fe_2S_2Cl_2]^-$ Anions [P(H) and P(L)], the Fission Intermediates [I1(L) and I2(L)], and the Fission Transition States [TS(H), TS1(L), and TS2(L)]**

	R ($S=0$)	P(H) ($S=^9/_2$)	P(L) ($S=^1/_2$)	TS(H) ($S=0$)	I1(L) ($S=0$)	TS1(L) ($S=0$)	I2(L) ($S=0$)	TS2(L) ($S=0$)
				a. Mülliken Charges				
Fe_{ox}	+0.57	+0.64	+0.80	+0.67	+0.67	+0.70	+0.75	+0.84
Fe_{red}	+0.57	+0.64	+0.45	+0.67	+0.55	+0.54	+0.51	+0.44
S_{ox}	−0.56	−0.64	−0.40	−0.64	−0.54	−0.62	−0.64	−0.60
S_{red}	−0.56	−0.64	−0.40	−0.64	−0.62	−0.59	−0.58	−0.62
Cl_{ox}	−0.51	−0.51	−0.51	−0.53	−0.49	−0.49	−0.48	−0.50
Cl_{red}	−0.51	−0.51	−0.54	−0.53	−0.52	−0.55	−0.55	−0.56
				b. Net Spin Densities				
Fe_{ox}	+3.86	+3.96	+3.99	+3.96	+4.02	+3.99	+3.97	+3.99
Fe_{red}	−3.86	+3.96	−3.57	−3.96	−3.82	−3.68	−3.62	−3.57
S_{ox}	+0.14	+0.43	+0.26	+0.43	+0.00	−0.03	−0.01	+0.26
S_{red}	−0.14	+0.43	+0.26	−0.43	+0.15	+0.25	+0.25	+0.26
Cl_{ox}	+0.11	+0.11	+0.12	+0.10	+0.14	+0.14	+0.15	+0.13
Cl_{red}	−0.11	+0.11	−0.07	−0.10	−0.09	−0.07	−0.06	−0.06

The Fe−Cl and Fe−S bond distances increase in the order of $Fe^{3+} < Fe^{2.5+} < Fe^{2+}$. The folded P(H) is a direct consequence of the delocalized minority spin, which has strong Fe−Fe σ bonding character. Analyses of the molecular orbitals and the spin densities show that the majority and minority spin Fe 3d orbitals of P(H) are entirely delocalized over both Fe centers, whereas those of P(L) are localized on the individual Fe sites with antiferromagnetic coupling (Table 2). In particular, the minority spin of P(H) is delocalized on the Fe−Cl β spin antibonding orbital with strong Fe($d_{x^2-y^2}$)−Fe($d_{x^2-y^2}$) σ bonding character, whereas the minority spin of P(L) is localized on the Fe−Cl antibonding orbital with very strong Fe d_{z^2} character. Because the energy difference between P(L) and P(H) can be attributed to a competition between HDvV spin coupling and resonance delocalization, the bonding interactions of the antiferromagnetically coupled [2Fe−2S] binuclear site in P(L) are larger than those of the ferromagnetically coupled [2Fe−2S] site with spin delocalization in P(H), contrary to the $[4Fe−4S]^{2+}$ cubane core. Overall, our DFT calculations show that P(L) is more stable than P(H) by 0.58 eV at the B3LYP/6-31(++)$_S$** level and by 0.89 eV when the spin-projection correction is taken into account.

Upon oxidation from $[Fe_2S_2Cl_2]^-$ to $[Fe_2S_2Cl_2]^0$, the Fe−Fe spin coupling interaction and Coulomb repulsion of the oxidized species $P_{oxd}(L)$ and $P_{oxd}(H)$ increase. In comparison to P(L), the Fe−Fe distance of $P_{oxd}(L)$ only shortens by 0.01 Å, indicating that the Fe−Fe antiferromagnetic coupling interaction partially counteracts the strong Coulomb repulsion of the ferric−ferric centers. With the increase in charge of the former ferrous center (+0.31 e) and the Cl atom (−0.18 e) upon the oxidation, average Fe−S bond distances and the Fe−Cl bond distances of $P_{oxd}(L)$ shorten relative to those of P(L) by 0.03 and 0.08 Å, respectively. On the other hand, the Fe−Fe distance of $P_{oxd}(H)$ significantly increases by 0.48 Å with respect to P(H) and P_{oxd}-(H) becomes planar because there is no longer strong Fe−Fe bonding from a delocalized minority spin and the ferromagnetic coupling interaction and the Coulomb repulsion of the ferric−ferric centers increase. In comparison to $P_{oxd}(L)$, the Fe−S and Fe−Fe bonds of $P_{oxd}(H)$ are longer by 0.06 and 0.31 Å, respectively (Figure 3). It indicates that the ferromagnetically coupling interaction of $P_{oxd}(H)$ decreases the bonding interactions between the iron centers and the ligands. Consequently, $P_{oxd}(H)$ is less stable by 0.85 eV than $P_{oxd}(L)$. Therefore, the

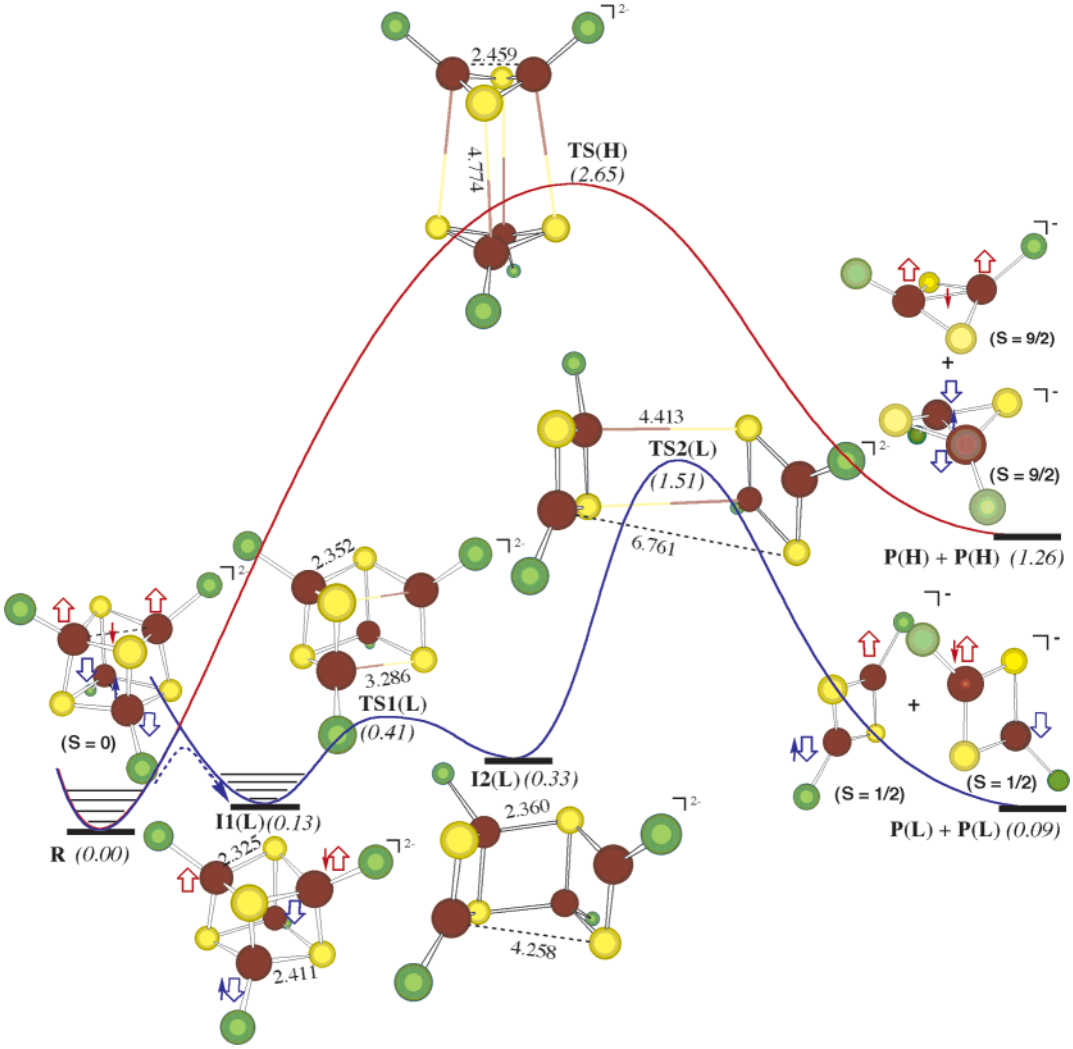

Figure 3. B3LYP/6-31G** optimized relative energies (eV, in parentheses) of the $[Fe_4S_4Cl_4]^{2-}$ fission including the SIE correction along the high-spin channel indicated by red curve in which the transition state and products are denoted by an H in parentheses and the low-spin channel indicated by blue curve in which the transition state, intermediates and products are denoted by an L in parentheses. Relevant B3LYP/6-31G** optimized bond lengths (Å) are also given for transition states and intermediates. The large hollow arrow represents the five majority spins (red for spin-up and blue for spin-down) and the small arrow represents the minority spin (red for spin-down and blue for spin-up).

major factor contributing to stabilization energy of the redox sites is the spin-coupling character of the system.

Overall, our DFT calculations support that the reduced $[Fe_2S_2Cl_2]^-$ species is a low-spin ground state, in which the minority spin has $Fe(d_{z^2})-Cl$ antibonding character. Further confirmation of the DFT results is made by the PES measurements. Our PES data revealed that the $[Fe_2S_2Cl_2]^-$ daughter anions have similar electronic structure to the $[Fe_4S_4Cl_4]^{2-}$ dianion, giving rise to an inverted level scheme. The B3LYP/6-31(++)$_S$G** calculations show that the calculated ADE and relaxation energy (λ_{oxd}) of the low-spin $[Fe_2S_2Cl_2]^-$ are 3.97 and 0.15 eV, respectively, in very good agreement with the experimental values of 3.80 and 0.13 eV (Table 1). On the other hand, a high-spin $[Fe_2S_2Cl_2]^-$ would have significant geometry distortions upon photodetachment of the delocalized electron, resulting in a larger ADE of 4.09 and a much larger λ_{oxd} of 0.64 eV, obviously inconsistent with the PES measurements. Although a more stable high-spin species of $[Fe_2S_2Cl_2]^-$ with $S = {}^7/_2$ is lower by 0.23 eV in energy than that of the $S = {}^9/_2$ state (through an α spin flip), the larger ADE of 4.22 eV and the larger λ_{oxd} of 0.27 eV of the $S = {}^7/_2$ state also disagree with the PES values.

Disassembly of $[Fe_4S_4Cl_4]^{2-}$. After confirming that the fission products are the low-spin $[Fe_2S_2Cl_2]^-$ anions [P(L)] and that the symmetric fission in $[Fe_4S_4Cl_4]^{2-}$ is almost thermoneutral, the next questions are how the fission reaction overcomes an expected large energy barrier arising from the breaking of four strong Fe−S bonds and whether it is possible that the fission proceeds via a high-spin channel and then the products decay to a low-spin species. To understand the kinetic behavior of the fission reactions, we performed B3LYP geometry optimizations and energy calculations to search for transition states and possible fission intermediates along the two fission channels.

(a) High-Spin Fission Channel of $[Fe_4S_4Cl_4]^{2-}$. Because the high-spin fission channel involves the breaking of four Fe−S bonds between the two antiferromagnetically coupled sublayers of $[Fe_4S_4Cl_4]^{2-}$, this channel would be expected have a lower barrier than the low-spin fission channel, which involves the breaking of two additional Fe−Fe bonding interactions within the two sublayers. We carefully searched the stationary points along the high-spin fission pathway and only found a late transition state TS(H) (Figure 3), in which the distance between the two sublayers is 4.774 Å and the structure of each sublayer already resembles that of the daughter anion P(H). In comparison to R, the Fe−Fe and Fe−S bond distances of TS(H) are shorter by 0.398 and 0.105 Å, respectively. The intracluster Coulomb repulsion, the increasing bonding interaction between the Fe

centers and ligands within the two sublayers, and the magnetic repulsion derived from the antiferromagnetic coupling between the two ferromagnetically coupled sublayers all play a role in this fission channel. This channel is endothermic by 1.26 eV with a high barrier of 2.95 eV. Taking the SIE correction and spin projection into account, the fission reaction is endothermic by 1.34 eV and the fission barrier is estimated to be ~2.7 eV, as shown in Figure 3. This fission channel is less endothermic per bond broken than the thiolate dissociation from the [1Fe] cluster (2 eV)[25] because the [2Fe−2S] daughter anions have stronger Fe−S and Fe−Fe bonding interactions than the [4Fe−4S] parent. However, the fission barrier is sufficiently high and the reaction is significantly endothermic so that this fission channel is expected to be unfavorable, indicating that a high-spin channel fission followed by decay to low-spin products is unlikely.

(b) Low-Spin Fission Channel of $[Fe_4S_4Cl_4]^{2-}$. The low-spin fission channel of $[Fe_4S_4Cl_4]^{2-}$ would appear to be favored over the high-spin channel on the basis of the low-spin state of the antiferromagnetically coupled $[Fe_2S_2Cl_2]^{-}$ daughter anions [P(L)]. Although the low-spin fission process is favored thermodymically over the high-spin fission process, if the low-spin fission of $[Fe_4S_4Cl_4]^{2-}$ proceeded through a symmetric fission transition state like in the high-spin channel, the reaction might encounter a higher activation energy than the high-spin channel because it involves the breaking of four strong Fe−S bonds and two additional Fe−Fe bonds. Such a high barrier for the low-spin channel might result in some high-spin products as well. However, because only low-spin $[Fe_2S_2Cl_2]^{-}$ products were observed experimentally, it suggests that there might be other low-barrier pathways along this fission channel.

Our calculations of the [1Fe] complexes suggest that the conversion of the high-spin tetrahedral ferrous site to the trigonal planar ferrous site is exothermic by ~2 eV with a low barrier of 0.5 eV.[25,44] Because a relatively stable three-coordinate ferrous center exists in the antiferromagnetic daughter anion P(L), we suspected that a low barrier pathway might be possible via an intermediate with ferrous centers. Indeed, we found a half-open and relatively low-energy $[Fe_4S_4Cl_4]^{2-}$ intermediate I2(L) with two tetrahedral ferric centers and two trigonal planar ferrous centers (Figure 3). This intermediate I2(L) is only 0.33 eV higher in energy than the parent R. Reoptimization of the cubane structure $[Fe_4S_4Cl_4]^{2-}$ along the reaction coordinate from I2(L) to R using the electron configuration state of I2(L) failed to directly recover the parent R. Instead, a new antiferromagnetically coupled $[Fe_4S_4Cl_4]^{2-}$ I1(L) with a localized core spin character was unexpectedly found through searching for stationary points. The vibrational frequency calculation of the optimized $[Fe_4S_4]^{2+}$ core of I1(L) indicates it is a local minimum. The intermediate I1(L) contains two regular ferric and two ferrous centers, $[(Fe^{2+})_2(Fe^{3+})_2S_4]^{2+}$, in which the Fe^{2+}−S bonds are longer by 0.035−0.118 Å and the Fe^{3+}−S bonds are shorter by 0.029−0.041 Å than the $Fe^{2.5+}$−S bonds in the parent R (Figure 1). It is somewhat surprising that the new intermediate I1(L) is only less stable by 0.13 eV than the parent $[Fe_4S_4Cl_4]^{2-}$ (R). Moreover, we found that the intermediate I1(L) exhibits distinctly different electronic structure in its spin state (Table 2). In the parent $[Fe_4S_4Cl_4]^{2-}$, the two minority electrons delocalize on the two ferromagnetic sublayers, resulting in additional stabilizing interactions beyond the HDvV antiferromagnetic coupling between the two ferromagnetic sublayers. In the intermediate I1(L), the resonance delocalization within the two ferromagnetic sublayers vanishes and the spin densities localize at each Fe site, shown as HOMO and LUMO in Figure 4, consequently, the four $Fe^{2.5+}$ sites are converted to two Fe^{3+} and two Fe^{2+} sites without spin flipping.

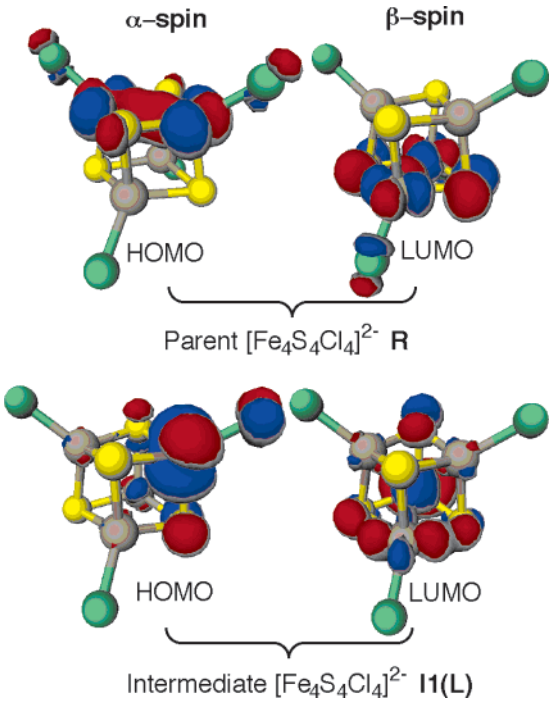

Figure 4. Molecular orbitals of HOMO and LUMO of the parent $[Fe_4S_4Cl_4]^{2-}$ (R) and the intermediate $[Fe_4S_4Cl_4]^{2-}$ [I1(L)].

Furthermore, a transition structure TS1(L) was found to connect the intermediates I1(L) and I2(L) with a low barrier of 0.28 eV. In the transition state TS1(L), the first step of fission starts within the Fe^{2+}−Fe^{2+} sublayer. The Fe^{2+}−S and Fe^{3+}−S bonding interactions on the two Fe^{2+}−Fe^{3+} sublayers of TS1(L) increase, whereas the Fe^{3+}−S bonding interactions in the Fe^{3+}−Fe^{3+} sublayer slightly decrease and the Fe^{2+}−S bonding interactions in the Fe^{2+}−Fe^{2+} sublayer decrease even more with respect to the intermediate I1(L). The breaking of the two Fe^{2+}−S bonds to a half-open intermediate I2(L) only leads to an endothermicity of 0.20 eV because of the increasing antiferromagnetic coupling within the two Fe^{2+}−Fe^{3+} sublayers. Upon breaking of the two Fe^{2+}−S bonds from the intermediate I2(L) to the final product P(L), we located another late transition state TS2(L), in which the distance of the breaking Fe^{3+}−S bonds is 4.413 Å and the two fragments are quite similar to the final daughter anions P(L). We note that the electron densities and spin densities of the ferric centers from the intermediate I2(L) through TS2(L) to the daughter anions P(L) do not significantly change. The reaction from I2(L) to P(L) is slightly exothermic by 0.24 eV with a barrier of 1.48 eV. Taking the SIE correction into account, the fission barrier is estimated to be ~1.2 eV. In the late stage of the fission reaction, with the decreasing Coulomb repulsion and increasing Fe−S bonding interactions, the total energy goes down. Overall, the reaction via the low-spin fission channel from the parent cluster R through the intermediates I1(L) and I2(L) to the daughter anions P(L) (Scheme 3) is almost thermoneutral with an endothermicity of only 0.09 eV with a lower barrier of 1.8 eV and, taking the SIE and spin projection corrections into account, is exothermic by 0.53 eV with a low barrier of 1.51 eV. Thus, this channel should be more favorable than the high-spin channel.

The proposal of conversion to an Fe^{II} before breaking the Fe−S bond is also consistent with previous studies of the [1Fe] complexes.[25] In these studies, we found that the thiolate association of $[Fe(SCH_3)_3]^0$ and the thiolate dissociation of

SCHEME 3

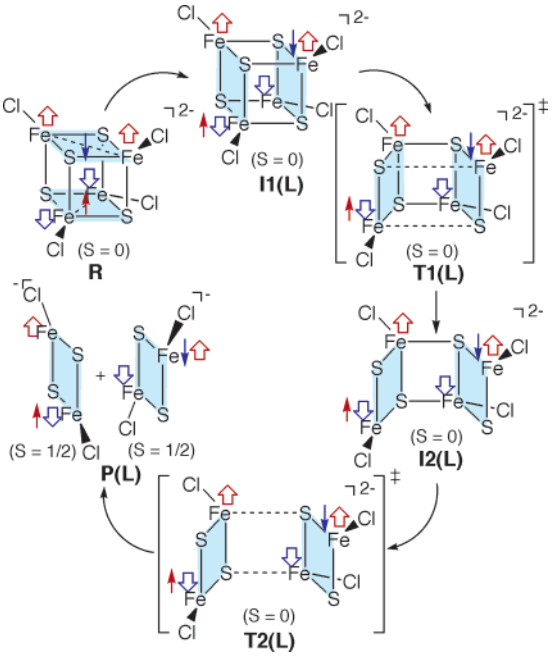

$[Fe(SCH_3)_4]^{2-}$ are exothermic by 2.6 and 1.8 eV, respectively, and the oxidation energies of $[Fe(SCH_3)_4]^{2-}$ and $[Fe(SCH_3)_3]^{-}$ are −1.7 and 2.7 eV, respectively, at the B3LYP/6-31(++)$_S$G** level of calculation. These results indicate that $[Fe(SCH_3)_4]^{n-}$ favors a high-spin d^5 electron configuration of Fe^{III}, whereas $[Fe(SCH_3)_3]^{n-}$ favors a high-spin d^6 electron configuration of Fe^{II}, which means that there must be a conversion from Fe^{III} to Fe^{II} upon dissociation of a thiolate ligand. The DFT calculations and experimental observations here show that in the gas phase the $Fe^{II} \leftrightarrow Fe^{III}$ conversion through spin-state crossovers with or without spin flipping, which would significantly lower the reaction barrier, may be involved in iron−sulfur cluster assembly/disassembly. Although a tetrahedral ferric center has a very low reduction potential in the gas phase, resulting in a ferrous center with high energy, the electrostatic effects in solvent or protein environments may significantly increase the reduction potentials of the tetrahedral ferric center, facilitating the $Fe^{III} \leftrightarrow Fe^{II}$ conversion. This means that the cluster can make contact quickly with a reactant or other redox site and provide or absorb electrons, making iron−sulfur cluster assembly/disassembly easier than in the gas phase.

Conclusions

The electronic structures, energetics, and fission mechanisms of the [4Fe−4S] analogue complexes have been investigated by DFT calculations and PES measurements. The results of these studies show that the spin crossover of the spin-delocalized cubane $[4Fe-4S]^{2+}$ cluster to the spin-localized $[4Fe-4S]^{2+}$ intermediate plays an important role in the symmetric fission of [4Fe−4S] analogue complexes.

Generally, the energy difference between the low-spin and high-spin states of [2Fe−2S] clusters can be attributed to a competition between HDvV spin coupling interaction and electron exchange interaction. The DFT optimized geometries show that the spin-coupling interaction of both the reduced $[Fe_2S_2Cl_2]^{-}$ site and the oxidized $[Fe_2S_2Cl_2]^{0}$ site is stronger than the electron exchange interaction. The low-spin states of $[Fe_2S_2Cl_2]^{-/0}$ are more stable by 0.89 and 0.79 eV, respectively, than the corresponding high-spin states of $[Fe_2S_2Cl_2]^{-/0}$. Thus, the low-spin fission products are favored thermodymically over the high-spin fission ones. Our DFT calculations suggest that the fission $[Fe_2S_2Cl_2]^{-}$ daughter cluster is a low-spin ground state in which the minority α spin has $Fe(d_{z^2})-Cl$ antibonding character, as is consistent with most findings for [2Fe−2S] clusters in previous experimental and theoretical studies. Further confirmation of the DFT results is made by the PES measurements. The B3LYP/6-31(++)$_S$G** calculations show that the calculated ADE and relaxation energy (λ_{oxd}) of the low-spin $[Fe_2S_2Cl_2]^{-}$ are 3.97 and 0.15 eV, respectively, in very good agreement with the experimental values of 3.80 and 0.13 eV (Table 2). However, the high-spin $[Fe_2S_2Cl_2]^{-}$, with significant geometry distortions upon photodetachment of the delocalized electron, has a larger ADE of 4.09 and a much larger λ_{oxd} of 0.64 eV, which is not in agreement with the PES measurements.

Full geometry optimizations and energy calculations of the $[Fe_4S_4Cl_4]^{2-}$ fission along the high-spin and low-spin fission pathways were performed at the B3LYP/6-31G** and B3LYP/6-31(++)$_S$G**//B3LYP/6-31G** levels. We found that the symmetric fission along the high-spin fission channel is endothermic by 1.34 eV with a very high barrier of 2.65 eV whereas the reaction along the low-spin fission channel in the gas phase is exothermic by 0.53 eV with a relatively low barrier of 1.51 eV. Significantly, the low barrier along the low-spin fission channel is due to a pathway through a spin-localized cubelike $[Fe_4S_4Cl_4]^{2-}$ intermediate, which contains two valence-localized Fe^{3+} sites and two valence-localized Fe^{2+} sites and is only 0.13 eV higher in energy than the parent. Further fission can easily proceed through breaking two tetrahedral $Fe^{2+}-S$ bonds to generate a half-opened intermediate. Thus, a low-energy conversion from sublayers with $Fe^{2.5+}-Fe^{2.5+}$ to $Fe^{2+}-Fe^{3+}$ reduces the strength of the Fe−S bonds within each sublayer even below the Fe−S bond between the sublayers so that the fission occurs by breaking both sublayers rather than occurring between the sublayers.

The current study provides valuable insight into iron−sulfur cluster assembly/disassembly mechanisms. The results show that symmetric fission of the isolated cluster occurs via spin localization of iron valences before fission. This implies that the mechanism can be tested experimentally (in conjunction with theoretical study) by altering the terminal ligands and/or second shell to change spin localization of [4Fe−4S] sites. Moreover, this implies a protein may be able to alter the favorability of different modes of fission by changes the degree of spin localization via altering the second shell.

Acknowledgment. This work was supported by grants from the National Institute of Health (GM45303 to T.I. and GM63555 to L.S.W.). S.N. thanks Dr. Mingliang Tan for helpful discussion about solvation effects. T.I. thanks Dr. Bernard R. Brooks at the National Heart, Lung, and Blood Institute, NIH, for his hospitality during the completion of this manuscript. Computing time was partially provided through grants from the National Science Foundation-National Partnership for Advanced Computational Infrastructure (MCB990010) and from the Molecular Science Computing Facility in the William R. Wiley Environmental Molecular Sciences Laboratory at the Pacific Northwest National Laboratory (PNNL), sponsored by the Office of Biological and Environmental Research of the U.S. Department of Energy. PNNL is a multiprogram national laboratory operated for the U.S. Department of Energy by Battelle Memorial Institute under contract DE-AC06-76RLO 1830.

References and Notes

(1) Gray, H. B.; Ellis, W. R., Jr. Electron Transfer. In *Bioinorganic Chemistry*; Bertini, I., Gray, H. B., Lippard, S. J., Valentine, J. S., Eds.; University Science Books: Mill Valley, CA, 1994; p 315.

(2) Cammack, R. *Adv. Inorg. Chem.* **1992**, *38*, 281.
(3) Tsibris, J. C. M.; Woody, R. W. *Coord. Chem. Rev.* **1992**, *38*, 281.
(4) Beinert, H.; Holm, R. H.; Münck, E. *Science* **1997**, *277*, 653.
(5) Beinert, H. *J. Bioinorg. Chem.* **2000**, *5*, 2.
(6) Flint, D. H.; Allen, R. M. *Chem. Rev.* **1996**, *96*, 2315.
(7) Beinert, H.; Kennedy, M. C.; Stout, C. D. *Chem. Rev.* **1996**, *96*, 2335.
(8) Rawls, R. L. *C&E News* **2000**, *78*, 43.
(9) Kiley, P. J.; Beinert, H. *FEMS Microbiol. Rev.* **1999**, *22*, 341.
(10) Moura, J. J. G.; Moura, I.; Kent, T. A.; Lipscomb, J. D.; Huynh, B. H.; LeGall, J.; Xaver, A. V.; Münck, E. *J. Biol. Chem.* **1982**, *257*, 6359.
(11) Kent, T. A.; Dreyer, J.-L.; Kennedy, M. C.; Huynh, B. H.; Emptage, M. H.; Beinert, H.; Münck, E. *Proc. Natl. Acad. Sci. U.S.A.* **1982**, *79*, 1096.
(12) Anderson, G. L.; Howard, J. B. *Biochemistry* **1984**, *23*, 2118.
(13) Khoroshilova, N.; Popescu, C. V.; Münck, E.; Beinert, H.; Kiley, P. J. *Proc. Natl. Acad. Sci. U.S.A.* **1997**, *94*, 6087.
(14) (a) Duin, E. C.; Lafferty, M. E.; Crouse, B. R.; Allen, R. M.; Sanyal, I.; Flint, D. H.; Johnson, M. K. *Biochemistry* **1997**, *36*, 11811. (b) Ollagnier-de Choudens, S.; Sanakis, Y.; Hewitson, K. S.; Roach, P.; Baldwin, J. E.; Münck, E.; Fontecave, M. *Biochemistry* **2000**, *39*, 4165. (c) Ugulava, N. B.; Gibney, B. R.; Jarrett, J. T. *Biochemistry* **2001**, *40*, 8343. (d) Ugulava, N. B.; Surerus, K. K.; Jarrett, J. T. *J. Am. Chem. Soc.* **2002**, *124*, 9050. (e) Tse Sum Bui, B.; Benda, R.; Schunemann, V.; Florentin, D.; Trautwein, A. X.; Marquet, A. *Biochemistry* **2003**, *42*, 8791.
(15) (a) Fu, W. G.; Morgan, T. V.; Mortenson, L. E.; Johnson, M. K. *FEBS Lett.* **1991**, *284*, 165. (b) Ryle, M. J.; Lanzilotta, W. N.; Seefeldt, L. C. Scarrow, R. C.; Jensen, G. M. *J. Biol. Chem.* **1996**, *271*, 1551.
(16) Sawers, R. G.; Zehelein, E.; Böck, A. *Arch. Microbiol.* **1988**, *149*, 240.
(17) (a) Khoroshilova, N.; Beinert, H.; Kiley, P. J. *Proc. Natl. Acad. Sci. U.S.A.* **1995**, *92*, 2499. (b) Beinert, H.; Kennedy, M. C. *Eur. J. Biochem.* **1989**, *186*, 5. (c) Plank, D. W.; Kennedy, M. C.; Beinert, H.; Howard, J. B. *J. Biol. Chem.* **1989**, *264*, 20385.
(18) Popescu, C. V.; Bates, D. M.; Beinert, H.; Münck, E.; Kiley, P. J. *Proc. Natl. Acad. Sci. U.S.A.* **1998**, *95*, 13431.
(19) (a) Monard, G.; Merz, Jr. K. M.*Acc. Chem. Res.* **1999**, *32*, 904. (b) Sigfridsson, E.; Olsson, M. H. M.; Ryde, U. *Inorg. Chem.* **2001**, *40*, 2509.
(20) Cambray, J.; Lane, R. W.; Wedd, A. G.; Johnson, R. W.; Holm, R. H. *Inorg. Chem.* **1977**, *16*, 2565.
(21) Yang, X.; Wang, X. B.; Wang, L. S. *Int. J. Mass. Spectrom.* **2003**, *228*, 797.
(22) Yang, X.; Wang, X. B.; Niu, S.; Pickett, C. J.; Ichiye, T.; Wang, L. S. *Phys. Rev. Lett.* **2002**, *89*, 163401.
(23) Wang, X. B.; Niu, S.; Yang, X.; Ibrahim, S. K.; Pickett, C. J.; Ichiye, T.; Wang, L. S. *J. Am. Chem. Soc.* **2003**, *125*, 14072.
(24) Wang, X. B.; Wang, L. S. *J. Chem. Phys.* **2000**, *112*, 6959.
(25) Niu, S.; Wang, X. B.; Nichols, J. A.; Wang, L. S.; Ichiye, T. *J. Phys. Chem. A* **2003**, *107*. 2898.
(26) Robin, M. B.; Day, P. *Adv. Inorg. Chem. Radiochem.* **1967**, *10*, 247.
(27) (a) Noodleman, L.; Baerends, E. J. *J. Am. Chem. Soc.* **1984**, *106*, 2316. (b) Noodleman, L.; Case, D. A. *Adv. Inorg. Chem.* **1992**, *38*, 423. (c) Mouesca, J.-M.; Chen, J. L.; Noodleman, L.; Bashford, D.; Case, D. A. *J. Am. Chem. Soc.* **1994**, *116*, 11898. (d) Noodleman, L.; Peng, C. Y.; Case, D. A.; Mouesca, J.-M.. *Coord. Chem. Rev.* **1995**, *144*, 199. (e) Torres, R. A.; Lovell, T.; Noodleman, L.; Case, D. A. *J. Am. Chem. Soc.* **2003**, *125*, 1923.
(28) (a) Noodleman, L. *Inorg. Chem.* **1988**, *27*, 3677. (b) Noodleman, L.; Case, D. A.; Baerends, E. J. in *Density Functional Methods in Chemistry*; Labonowski, J. K.; Andzelm, J. W. Ed.; Springer-Verlag: New York, 1991, p109.
(29) (a) Crouse, B. R.; Meyer, J.; Johnson, M. K. *J. Am. Chem. Soc.* **1995**, *117*, 9612. (b) Achim, C.; Golinelli, M.-P.; Bominaar, E. L.; Meyer, J.; Münck, E. *J. Am. Chem. Soc.* **1996**, *118*, 8168.
(30) Niu, S.; Hall, M. B. *Chem. Rev.* **2000**, *100*, 353.
(31) Yang, X.; Niu, S.; Wang, X. B.; Ichiye, T.; Wang, L. S. *J. Chem. Phys.* **2003**, *119*, 8311.
(32) Parr, R. G.; Yang, W. *Density-Functional Theory of Atoms and Molecules*; Oxford University Press: Oxford, U.K., 1989.
(33) (a) Becke, A. D. *Phys. Rev.* **1988**, *A38*, 3098. (b) Becke, A. D. *J. Chem. Phys.* **1993**, *98*, 1372. (c) Becke, A. D. *J. Chem. Phys.* **1993**, *98*, 5648. (d) Lee, C.; Yang, W.; Parr, R. G. *Phys. Rev.* **1988**, *B37*, 785.
(34) (a) Rassolov, V.; Pople, J. A.; Ratner, M.; Windus, T. L. *J. Chem. Phys.* **1998**, *109*, 1223. (b) Francl, M. M.; Petro, W. J.; Hehre, W. J.; Binkley, J. S.; Gordon, M. S.; DeFrees, D. J.; Pople, J. A. *J. Chem. Phys.* **1982**, *77*, 3654. (c) Hariharan, P. C.; Pople, J. A. *Theor. Chim. Acta* **1973**, *28*, 213.
(35) Noodleman L. *J. Chem. Phys.* **1981**, *74*, 5737.
(36) (a) Simons, J. Jorgensen, P. Taylor, H. Ozment, J. *J. Phys. Chem.* **1983**, *87*, 2745. (b) Bannerjee, A.; Adams, N.; Simons, J.; Shepard, R. *J. Phys. Chem.* **1985**, *85*, 52.
(37) (a) Clark, T.; Chandrasekhar, J.; Schleyer, P. v. R. *J. Comput. Chem.* **1983**, *4*, 294. (b) Krishnam, R.; Binkley, J. S.; Seeger, R.; Pople, J. A. *J. Chem. Phys.* **1980**, *72*, 650. (c) Gill, P. M. W.; Johnson, B. G.; Pople J. A.; Frisch, M. J. *Chem. Phys. Lett.* **1992**, *197*, 499.
(38) Niu, S.; Nichols, J. A.; Ichiye, T. Unpublished work.
(39) (a) Perdew, J. P.; Zunger, A. *Phys. Rev. B* **1981**, *23*, 5048. (b) Perdew, J. P. In *Density Functional Methods in Physics*; Dreizler, R. M., Ed.; Plenum: New York, 1985; p 265. (c) Perdew, J. P.; Ernzerhof, M. In *Electronic Density Functional Theory: Recent Progress and New Directions*; Dobson, J. F., Vignale, G., Das, M. P., Eds.; Plenum: New York, 1997, p137.
(40) High Performance Computational Chemistry Group, *NWChem, A Computational Chemistry Package for Parallel Computers, Version 4.5*; Pacific Northwest National Laboratory, Richland, WA 99352, 2003.
(41) Black, G.; Chase, J.; Didier, B.; Feller, D.; Gracio, D.; Jones, D.; Jurrus, E.; Keller, T.; Matsumoto, S.; Mendoza, E.; Nordwall, D.; Olander, M.; Palmer, B.; Peden, N.; Schuchardt, K.; Stephan, E.; Taylor, H.; Thomas, G.; Vorpagel, E.; Windus, T. *Ecce, A Problem Solving Environment for Computational Chemistry, Software Version 1.5*; Pacific Northwest National Laboratory, Richland, WA 99352-0999, 2000.
(42) Bertini, I.; Cicurli, S.; Luchinat, C. *Struct. Bond.* **1995**, *83*, 1.
(43) (a) Middleton, P.; Dickson, D. P. E.; Johnson, C. E.; Rush, J. D. *Eur. J. Biochem.* **1978**, *88*, 135. (b) Papaefthymious, V.; Millar, M. M.; Münck, E. *Inorg. Chem.* **1986**, *25*, 3010. (c) Angrove, H. C.; Yoo, S. J.; Burgess, B. K.; Münck, E. *J. Am. Chem. Soc.* **1997**, *119*, 8730. (d) Yoo, S. J.; Angrove, H. C.; Burgess, B. K.; Hendrich, M. P.; Münck, E. *J. Am. Chem. Soc.* **1999**, *121*, 2534.
(44) The B3LYP/6-31G** energy profiles in the gas-phase show that the dissociation of $[Fe^{II}Cl_4]^{2-}$ to $[Fe^{II}Cl_3]^-$ and Cl^- is exothermic by 1.9 eV with a low barrier of 0.5 eV, whereas the dissociation of $[Fe^{III}Cl_4]^-$ to $[Fe^{III}Cl_3]^0$ and Cl^- is very endothermic by 3.6 eV without a transition state because of the stronger Fe^{III}−Cl bonding.